J Mater Sci: Mater Electron
DOI 10.1007/s10854-015-2701-4

REVIEW

Photoluminescence of $BaZrO_3$ explained by a order/disorded transformation

E. C. Aguiar · A. Z. Simões · C. A. Paskocimas · M. Cilense · E. Longo · J. A. Varela

Received: 24 September 2014 / Accepted: 16 January 2015

Abstract A hydrothermal (HTMW) microwave method was used to synthesize ordered–disordered $BaZrO_3$ (BZ) nanoparticles at temperature of 140 °C with times ranging from 15 min to 2 h. X-ray diffraction results verified the formation of BZ crystallites at a soaking time of 2 h while infrared data showed no traces of carbonate. Field emission scanning microcopy revealed a homogeneous size distribution of nanometric BZ powders. HTMW produced nanoparticles of pure BZ phase, with a size ranging from 40 to 80 nm. These results are in agreement with Raman scattering values which show that the HTMW synthesis route is rapid and cost effective. This method could be used as an alternative to obtain BZ nanoparticles as compared to other chemical methods. Intense photoluminescence in disordered BZ powders was observed at room temperature. The key of mystery of the intense PL emission is related to order–disorder structural in BZ lattice.

E. C. Aguiar · C. A. Paskocimas
Departamento de Ciência E Engenharia de Materiais, Universidade Federal do Rio Grande do Norte, Natal, RN CEP 14800-900, Brazil

A. Z. Simões (✉)
Faculdade de Engenharia de Guaratinguetá, Universidade Estadual Paulista - UNESP, Av. Dr. Ariberto Pereira da Cunha, 333, Bairro Pedregulho, Guaratinguetá, SP CEP 12516-410, Brazil
e-mail: alezipo@yahoo.com

M. Cilense · E. Longo · J. A. Varela
Laboratório Interdisciplinar em Cerâmica (LIEC), Departamento de Físico-Química, Instituto de Química, UNESP, Araraquara, SP CEP 14800-900, Brazil

1 Introduction

Recently, several studies have been performed, especially in $BaTiO_3$ perovskite due to their excellent optical and electrical properties [1–3]. One attraction of this range of the visible spectrum is that the short wavelength permits higher density optical storage devices, as is evident in the latest generation of DVD players that are currently emerging. Another is the possibility of high-efficiency, long-lifetime, solid-state lighting using the blue to complement existing longer-wavelength sources for white lighting [4]. There are few studies of photoluminescence (PL) in zirconates; especially those with visible emission region are reported in literature [5]. The $BaZrO_3$ (BZ) crucibles fabricated from powders synthesized by solid-state reaction of $BaCO_3$ and ZrO_2 were successfully used for $YBa_2Cu_3O_7$ crystal growth by Erb et al. [6] and by Liang et al. [7]. The literature also reports another applications for this material in several areas. In aero-space and related industries with excellent thermomechanical properties [8], solid oxide fuel cells and sensors that is a proton type conductor [9–13]. Several methods have been employed to prepare metal zirconates such as co-precipitation/calcinations, [11] sol–gel, [12] polymeric precursor, [13, 14] and single-step combustion [15]. However, some of these synthetic procedures still require a calcination treatment to transform a homogeneous precursor into a crystalline oxide phase. For BZ, sol–gel oxalate or citrate routes produce powders with very small grain size; however, many of these methods require organic solvents, which must be recycled [16, 17]. Recently, the possibility of obtaining submicron crystalline BZ by precipitation in an aqueous basic solution below 100 °C has been examined by Boschini et al. [18] while hydrothermal synthesis has been developed over the last decades in order to obtain

Published online: 13 February 2015

nanometric BZ powders [19] using faster and less expensive methods. In addition, microcrystalline [20] and nanometric BZ powders were obtained using a hydrothermal synthesis method, working under supercritical conditions. Lu et al. [21] discussed the evolution of the architecture of BZ from a truncated dodecahedral shape into a spherical shape as ethanol content is increased along a conventional hydrothermal route. Moreover, these authors suggested a feasible shape-dependent PL emission for Eu-doped BZ microcrystals. Komarmeni et al. [22] have introduced the microwave assisted hydrothermal (HTMW) method for the synthesis of several electro-ceramic powders, as a genuine low temperature, fast reacting and environmentally friendly method. [23] A year later the same authors developed the synthesis of perovskite oxides for BZ-based materials with spherical morphologies and a particle size in the range of 0.1–0.5 mm. Recently, the use of microwave heating was proven to be effective for ceramic compounds in the field of powder preparation with both expected and unexpected merits: e.g., kinetic enhancement, low reaction temperature, time reduction, control of the overall particle size and aggregation process as well as new and interesting properties. [22–31] On the other hand, further research by our group has significantly expanded our efforts to demonstrate that the MWHT method is one of the most efficient, versatile, and highly cost-effective approaches to obtain crystalline, single-phase micro and/or nanoscale materials at lower temperatures and shorter reaction times but with little residual impurities (normally <1 ppm) [29–32]. The low cost and convenience of the process, good reproducibility, high yield and clean reactions of the present synthetic method provide an incentive to scale it up for industrial production. Several studies were performed using template-directed approaches which have been demonstrated to be effective for the preparation of many materials using various synthetic methods (including HTMW heating) that often involve the coating of crystals on the template surface, followed by removal of the template [33, 34]. In particular, polymer-metal oxide nanocomposites are currently of considerable interest as solution processable high-permittivity materials for electronic applications such as embedded, multilayer and high-energy-density capacitors, and gate insulators in organic field effect transistors [35–39]. In addition, colloidal nanocrystals stabilized by a layer of surfactants attached to their surface are synthesized with finer control over nanocrystal growth. [40]. The different synthetic methods used in the preparation of BZ powders suggest the formation of different defects which can be indicative of different conformations in the cubic structure during BZ growth.

In this respect, the PL emission of semiconductors is an important material property because it can provide information on defects and relaxation pathways of excited states depending upon preparation techniques. In this work, we report a detailed study on the effect of soaking time on the growth of BZ nanoparticles. The research involves three critical steps: (1) synthesis of shape controlled crystals; (2) the structural characterization with PL, field-emission scanning electron microscopy (FE-SEM), X-ray diffraction (XRD) and Fourier transform Raman spectroscopy (FT-Raman); and finally (3) an investigation of PL emission.

2 Experimental procedure

The preparation of BZ powders using the HTMW method was systematically investigated. Each precursor was properly dissolved in distilled water to stoichiometric proportions appropriate for each sample. This dissolution was performed under vigorous stirring with subsequent addition of KOH 6 M for the precipitation of hydroxides reaching a pH $\approx$ 14. The mixture was ultrasonically dispersed for 10 min, transferred into a sealed Teflon autoclave and then placed in a adapted microwave furnace (Panasonic, Model MN-S46B, 800 W) with a frequency of 2.45 GHz and variable power up to 300 W. The temperature inside the vessel was controlled through an optical fiber sensor (Model EST-300-CEM Corp.). The hydrothermal treatment was performed at the same temperature for different soaking times. The reactions were carried out for 15 min to 2 h at a temperature of 140 °C, which can generate pressures up to 4 Bar. After the hydrothermal reaction, the autoclave was naturally cooled to room temperature. The resulting powders (insoluble in water) were separated by centrifugation and washed with de-ionized water in sequence to remove all soluble salts, and then dried in an conventional oven at 80 °C for 24 h in atmosphere. The powders obtained were characterized by X-ray powder diffraction (XRD) using a (Rigaku-DMax/2500PC, Japan) with Cu-Kα radiation ($\lambda = 1.5406$ Å) at 0.02°/min^{-1}. The crystallite size (d) of BZO was calculated using Scherrer equation $d = k\lambda/\beta \cos\theta$, where k is constant, λ is wavelength of X-rays and β is the full width at half maximum (FWHM) for main reflection measured from slow scan where θ is the diffraction angle of the main peak. The periodic DFT calculations with the B3LYP hybrid functional [16, 17] have been carried out by means of the CRYSTAL03 computer code [41]. This functional has already been successfully employed in the electronic and structural properties of various compounds on the bulk form [19]. The atomic centers have been described by all electron basis sets 9763-311(d631)G* for Ba, 976-31(d62)G* for Zr and 6-31G* for O atoms [20].

Infrared spectroscopy (Model 400-IR/FT, IMPACT) was used to detect traces of impurities in barium zirconate powders. Raman spectra were collected (Bruker RFS-100/S

Raman spectrometer with Fourier transform); a 1064 nm YAG laser was used as the excitation source, and its power was kept at 150 mW. Microstructural characterization was performed by FE-SEM (Supra 35-VP, Carl Zeiss, Germany). The white solid product was washed with deionized water several times until neutral pH and dried at 60 °C. Measurements of PL emission were made using 350.7 nm (3.52 eV) exciting wavelength of a krypton ion laser (Coherent Innova) with an output power of the laser kept at 200 mW. All measurements were taken at room temperature.

3 Results and discussion

X-ray diffraction patterns of BZ nanoparticles annealed at different soaking times are shown in Fig. 1. The main characteristic peaks are in agreement with JCPDS 6-0399 standard for perovskite cubic phase of BZ, see Fig. 1d. However, besides BZ phase, diffraction peaks related to barium carbonate is evident which was formed due the dissolution of CO_2 from the air in the water as well as a non stoichiometry phase of $Zr_{0.952}O_2$. The crystallization

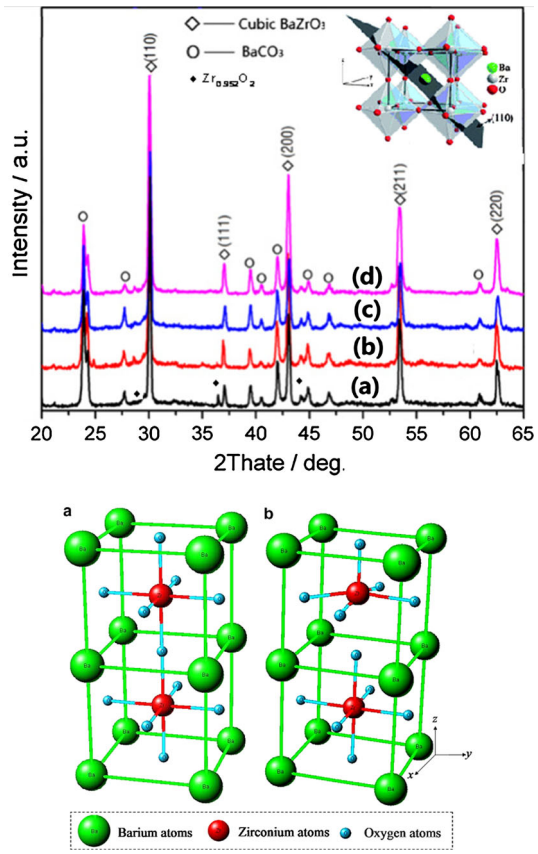

Fig. 1 X-ray diffraction patterns of $BaZrO_3$ ceramics synthesized at 140 °C-1 h for: (*a*) 15 min (*b*) 30 min (*c*) 60 min and (*d*) 120 min. Super-cell representation 1 × 1 × 2 of the cubic BZO structure: **a** ordered BZO-o and **b** disordered BZO-d

process of the structurally BZ clearly starts at a soaking time of 60 min (see Fig. 1c), and is completely ordered after 120 min. Moreover, the XRD pattern of the BZ annealed at lower soaking times indicates a disordered phase, being BZ phase structurally ordered with the rise of soaking time. The main (110) diffraction plane is related to the periodic arrangement of dodecahedral (BaO_{12}) and octahedral (ZrO_6) clusters. BZO presents a cubic perovskite-type structure in the crystalline form with space group Pm3m. The experimental value of the a lattice constant correspondent to the BZO crystalline phase is 4.167 Å. The lattice parameters were calculated using the least square refinement from the UNITCELL-97 program [21]. In a first step, an optimization procedure of the a lattice parameter has been carried out, yielding a value of 4.262 Å. From this optimized structure, we model a 1 × 1 × 2 supercell as a periodic model to represent the ordered BZO-o structure (see Fig. 1a). This ordered model can be designed as $[ZrO_6]/[ZrO_6]$, where each Zr atom is surrounded by six O atoms. The disordered BZO-d structure was represented by the displacement of one Zr atom in the [00 1] direction. This displacement is the simplest way to represent the two models of Zr, $[ZrO_5]$, square-base pyramid and $[ZrO_6]$ octahedron. Therefore, BZO-d structure can be designed as $[ZrO_6]/[ZrO_5]$ (see Fig. 1b). Crystallite sizes were estimated to be between 30 and 100 nm, depending on total soaking times. It is observed that crystallite size raised as overall soaking times increases, whereas diffraction intensity peaks increase as soaking time increases. This suggests better densification and crystallinity as well as strong powders agglomeration. It might also indicate the aggregation of crystallites in larger secondary particles [28, 29]. Figure 2 shows FTIR spectral features of BZ samples. Strong intense bands at 3,435, 1,589 cm^{-1} and below 700 cm^{-1} were observed. The intense bands at 3,435 and 1,589 cm^{-1} correspond to the ν (O–H) mode of (H-bonded) water molecules and δ (OH), respectively. Residual water and hydroxy group are usually detected in the as prepared samples regardless of synthesis method used [42] and further heat treatment is necessary for their elimination. The FTIR spectrum of the ceria also exhibits strong broad band below 700 cm^{-1} which is due to the δ (Ba–O–Zr) mode. Specifically, the strong absorptive peaks at 400–600 cm^{-1} was attribute to the Ba–O stretching and bending vibration, being characteristics of the tetrahedral BaO_{12} groups in the compounds. The hydroxylation and deprotonation of metal ions can be accelerated by raising the solution temperature or pressure [43]. No traces of impurties chemically bonded to the surface of the BZ nanoparticles was noted. The crystallized material was found to have OH^- ions due to the alkali used in the present reaction conditions. Furthermore, the hydroxyl content was found to change with the mineralizing agent

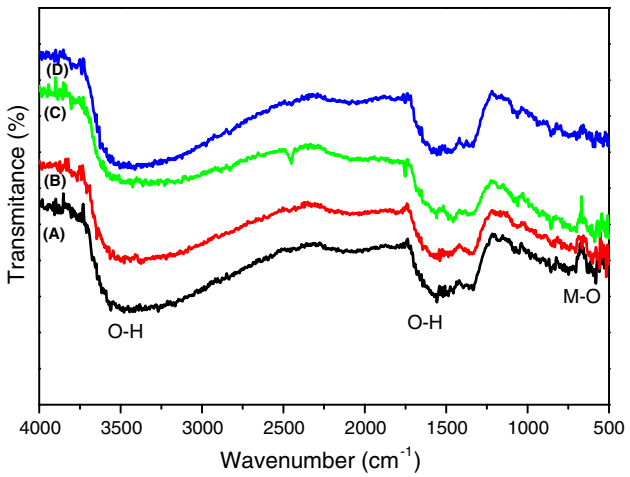

Fig. 2 FT-IR spectrum of $BaZrO_3$ ceramic powders synthesized at 140 °C-1 h for: (*a*) 15 min (*b*) 30 min (*c*) 60 min and (*d*) 120 min

who could be due to the vigorous action of microwaves to remove these groups at elevated temperatures during the hydrothermal process. In hydrothermal-microwave processing, the high frequency electromagnetic radiation interacts with the permanent dipole of the liquid (H_2O) which initiates rapid heating from the resultant molecular rotation. Also, permanent or induced dipoles in the dispersed phase cause rapid heating of the particles which results in a reaction temperature in excess of the surrounding liquid-localized superheating. Following the literature, hydrolysis refers to those reactions of metallic ions with water that liberate protons and produce hydroxide or oxide solids.

At room temperature, BZ has an ideal cubic perovskite structure. The signal collected for the cubic sample is thus to be ascribed to Raman-forbidden modes possibly activated by lattice disorder or second-order Raman scattering. In first-order Raman process, the phonon can only originated from a point near the zone center. Because all the zone-center optical phonons are of odd symmetry, no first-order Raman activity is expected on the basis of factor group symmetry analysis; instead the room temperature spectrum should be dominated by second-order scattering. Raman-active phonon modes can be employed to estimate the structural order at short-range of a material. The group theory calculation presents 26 different vibrations for the BZ, which is represented by Eq. (1)

$$\Gamma = 3Ag + 5Au + 5Bg + 3Bu + 5Eg + 5Eu \quad (1)$$

where all vibrations (Ag, Bg and Eg) are Raman-active, A and B modes are non-degenerate, whereas E modes are doubly degenerate. The subscribed 'g' and 'u' for even and odd, respectively, indicate the parity under inversion in centrosymmetric crystals. One A_u and one E_u correspond to the zero frequency of acoustic modes, the others are optic modes. The pairs of species enclosed in parenthesis arise from the same motion of the BZ molecule. In scheelites, the first member of the pairs (g) is a Raman-active mode and the second member (u) is active only in infrared (IR), except for the B_u silent modes that are not IR active. Consequently, we expect 13 zone-center Raman-active modes in BZ, as presented in Eq. (2)

$$\Gamma = 3Ag + 5Bg + 5Eg \quad (2)$$

To confirm the formation of pure BZ nanoparticles, FT-Raman spectrum was obtained (see Fig. 3). Because BZ nanoparticles were obtained under strong alkaline conditions, it is likely that residual hydroxyl groups were incorporated in the perovskite oxygen sublattice during the crystal growth as a result of the substitution of OH for O_2^-, other point defects such as cation vacancies or neutral vacancy pairs may also be created to maintain the electroneutrality of the perovskite structure. Figure 3 shows the room temperature Raman spectra of the BZ ranging from 50 to 1,200 cm^{-1}. The FT-Raman spectra consists of a band at three photon lines at around 85, 135, and 766 cm^{-1} that are ascribed to TO1, TO2, and TO4 first-order modes, respectively, and the second-order modes are ascribed at 222 and 556 cm^{-1}. In addition, the shifts at 153, 689 and 1,059 cm^{-1} (the $BaCO_3$ reference sample) as well as the vibrational mode correspond to distortions on the octahedral site of the zirconium inside the unit cell of the BZ structure [44].

FEG-SEM micrographs of BZ obtained at different soaking times are shown in Fig. 4. According to the image, most of the particles of BZ powders are homogeneous with an average particle size calculated from the FE-SEM images of around 40-100 nm as the soaking time increases. However, BZ powders obtained at lower soaking time reveal smaller particles which display poor

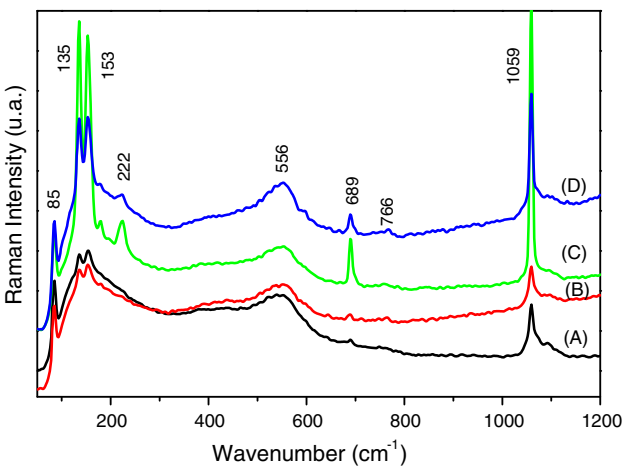

Fig. 3 Raman spectroscopy at room temperature of $BaZrO_3$ ceramics synthesized at 140 °C-1 h for: (**a**) 15 min, (**b**) 30 min (**c**) 60 min and (**d**) 120 min

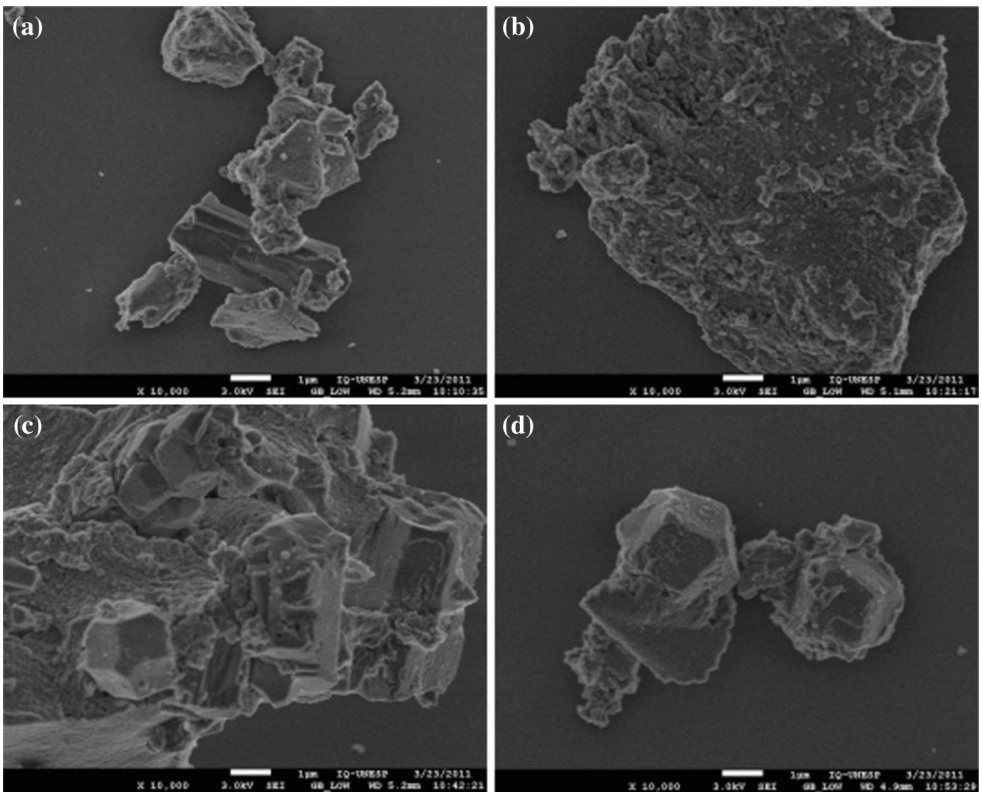

Fig. 4 FE-SEM micrographs of $BaZrO_3$ obtained at different soaking times: (**a**) 15 min, (**b**) 30 min (**c**) 60 min and (**d**) 120 min

contrast and intense agglomeration amongst extremely fine particles. The particle size tends to increase during the first minutes but no further evolution in particle size can be observed for reaction times longer than 60 min. The small size of the BZ particles synthesized at lower soaking time can be explained quite simply. It is postulated that at the start of the reaction a large number of nucleus forms in the solution and as the reaction takes place in a very dilute solution there is not enough reactant left for the growth of the particles. As a result, the particles do not grow beyond 100 nm. There was not obvious change in the morphology under different annealing conditions. The higher agglomeration degree after hydrothermal treatment can be explained by Van der Waal's forces. Moreover, the distribution in size seemed to be homogeneous and the shape appeared rounded. The synthesized BZ particles were relatively spherical with uniform size distribution, which was observed by FEG-SEM. Nanometric and isotropic BZ crystallites obtained in this study are quite different from the previous study, where BZ powders agglomerated into a cubic shape with the side size of 4.8 nm under hydrothermal conditions [45]. In the hydrothermal process, the soaking time was found to be essential. In our case, a critical soaking time could exist above which the formation of agglomerates was favored, and the formation of weak agglomerated BZ was highly dependent upon this formation. The "dissolution and crystallization" process can be utilized to describe the hydrothermal reaction [46]. During the hydrothermal treatment, Ba^{+2} or Zr^{+4} hydroxides underwent an attack by basic medium to dissolve and react at high temperatures and pressures, and then precipitated as insoluble ceramic oxide particles from the supersaturated hydrothermal fluid. If the temperature and pressure conditions are carefully maintained during the duration of the experiment, neither etching of BZ crystals nor the formation of agglomerates is observed. Therefore, the dissolution and crystallization process continued in supersaturated fluid in such a way that the system was self-stabilizing. We conjecture that the dissociation of barium/zirconium hydroxides and the formation of ionic complexes might prevent the growth of BZ crystallites and limit the size of particles to the nanometric range. The agglomeration process was attributed to Van der Waals forces. To reduce the surface energy, the primary particles have a tendency to form nearly spherical agglomerates, in a minimum surface to volume ratio [47]. This type of grain structure is common in oxide, ferrite and titanate ceramics [48, 49] which is a result of an abnormal/discontinuous grain particle and also called an exaggerated grain particle. In abnormal growth, some particles grow faster than others with increasing sintering temperature.

Abnormal grain particles may results from: (1) the existence of second phase precipitates or impurities, (2) materials with high anisotropy in interfacial energy and (3) materials with high chemical equilibrium [50]. In hydrothermally derived BZ which crystallizes in a cubic structure it can be assumed that the abnormal grain particles comes from factor (2) and (3) due the existence of high chemical equilibrium. The random aggregation process between the small particles can be related to an increase in effective collision rates between small particles by microwave radiation [51] which indicates that microwave energy favors an anisotropic growth caused by the differences in the surface energies on the different crystallographic faces [52]. Possibly, the imperfections or differences between the particles size can be associated with the influence of microwave energy during the BZ phase growth process.

UV–Vis spectroscopy measurements were evaluated in the BZ nanoparticles (see Fig. 5). The maximum absorption was located at around 473 nm with respective band gap values determined from the Kubelka Model [30]. The optical energy band gap is related to the absorbance and to the photon energy by the following equation:

$$h\nu\alpha \propto \left(h^{\circ} - \mathrm{E}_{\mathrm{g}}^{\mathrm{opt}}\right)^{2} \tag{3}$$

where α is the absorbance, h is the Planck constant, ν is the frequency and E_g^{opt} is the optical band gap [31]. The obtained values are 3.13, 3.18, 3.15, 3.20 eV, which are similar to the values reported by Parida et al. [24] (around 3.55 eV). These values are within the range already reported in the literature [22, 23] for pure BZ, 3.8–4.8 eV. Our BZ nanoparticles presented characteristic absorption spectra of ordered or crystalline materials. Geometrical alterations related to BO_6 and AO_{12} clusters in perovskite such as distortion, breathing and tilt, create a huge number of different materials properties. Both breathing and tilting of the BO_6 clusters necessarily induces a distortion of the AO_{12} clusters leading to a breaking symmetry process. Therefore, for ABO_3 perovskites, material properties can be primarily associated with polyhedral constituents and the mismatch of both clusters can induce structural order–

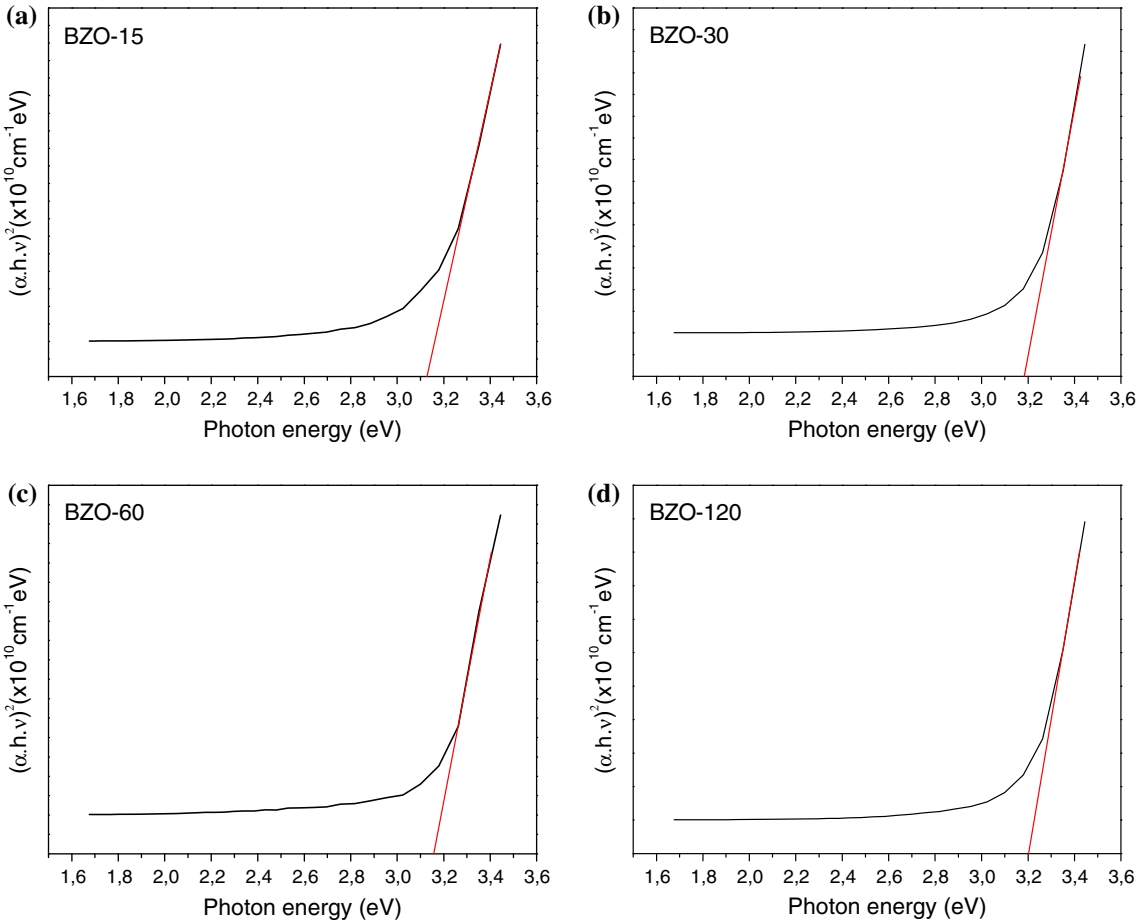

Fig. 5 UV–Vis absorbance spectrum of $BaZrO_3$ ceramic powders for several times of synthesis

disorder effect. These results indicate that the exponential optical absorption edge and the optical band gap are controlled by the degree of structural disorder in the BZ lattice. This increase in the band gap can be ascribed to a reduction of defects in the lattice which decreases the intermediary energy levels due to the reduction of oxygen vacancies located at BO_6 octahedra and AO_{12} clusters. The variations on band gap with increasing soaking times indicate different degrees of disorder within the BZ lattice [23]. In general it seems that the lower soaking time dramatically increases the disorder (reducing the band gap) and that slight additional soaking time help to recover some degree of order, and in turn the band gap increases. This also might be correlated with the reduction of the crystallites sizes as soaking time decreases, and the aggregation of such smaller crystallites in the larger micron sized faceted particles observed in Fig. 4. The main differences in optical band gaps can be related to the different factors, mainly including: synthesis method, shape (powder, crystal or thin film) and synthesis conditions.

Figure 6 shows PL spectra of BZ powders annealed at 140 °C at different soaking times. The intense green light PL emission at $\lambda = 480$ nm in BZ powders annealed at 15 min is associated with the structural order–disorder degree in BZ lattice. The presence of diffraction peaks can be used to evaluate long range structural order. BZ powder annealed at 140 °C for 2 h showed all diffraction peaks with a cubic perovskite-type structure in crystalline form while BZ powder annealed at 140 °C for 15 min present traces of secondary phases characteristic of long-range order–disorder. The emission band profile is a typical multiphonon process, i.e. a system in which the relaxation occurs by several paths, involving the participation of numerous levels within the perovskite band gap. Before donor excitations, a hole polaron in the acceptor state and an electron in donor

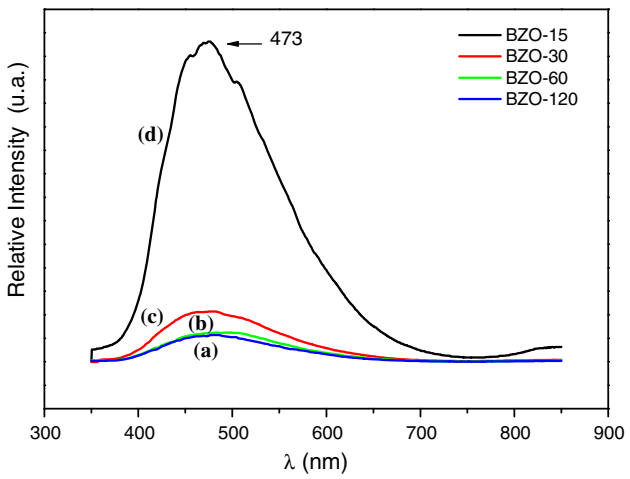

Fig. 6 PL emission spectrum at room temperature of $BaZrO_3$ ceramics synthesized at 140 °C-1 h for: (*a*) 15 min, (*b*) 30 min (*c*) 60 min and (*d*) 120 min

state are created according to the following equations. We believe that the formation of the $[ZrO_5]$–$[ZrO_6]$ clusters or to hole(h·)/electron(e′) pairs in order-disordered BZ structure presents important role for the PL emission. This clusters creates e′ and h· polarons that can be designed as Jahn–Teller bipolarons [19]. The absence of PL emission with increase of soaking time is caused by the structural organization of lattice with formation of $[ZrO5.Vo\cdot] + ½\ O_2 \rightarrow [ZrO6]$ after changes in the annealing conditions. Considerable studies have verified that the PL properties of perovskite oxides of group IV elements stemmed from oxygen vacancies and structural defects. Generally, the PL intensity was enhanced by the reduced particle sizes, due to the increased defects that were induced by the enlarged surface areas. Several groups have found that the PL intensities were directly related to the particle sizes of perovskite oxides [20, 37, 39]. The increased defects caused by the reduced particle sizes enhanced the PL intensities. The poorly crystallized powders supplied more oxygen vacancies to enhance the PL performance. Highly crystallized nanoparticles had fewer oxygen vacancies to trap photons. However, the samples with smaller particle size would pack better to increase the amount of materials being illuminated per set area, and the nature of the particles would likely result in a better penetration depth for the radiation to increase the actual volume (and thus the amount) of powders illuminated in the case of the more transparent powders. Moreira et al. [53] proposed a mechanism to promoted the formation of defects and/or distortion in the BZ polyhedrons. According to them the PL emission can be attributed to the freezing of structural defects inside the zirconium octahedrons (associated with both distortional octahedral (ZrO_6) and dodecahedral (BaO_{12}) clusters that form the constituent polyhedrons of the BZ system) which are related to the microwave energy acting directly on the rotational barriers of the water, providing a high heating rate and increase the self-assembled pressure, thus forcing the fast formation of distorted BZ quasi-crystalline BZ powders. A proposed model for wide band PL property is illustrated in Fig. 7. The most important events occur before excitation, i.e., before the photon arrives. Structural defects at short and intermediate-range leads to the formation of intermediary energy levels into the band gap and inhomogeneous charge distribution in the unit cell, allowing the trapping of electrons (see Fig. 7a). The lower conduction band is mainly due to the 4d orbitals of zirconium atoms. The levels responsible by the reduction of band gap are mainly due to 2p orbitals of oxygen atoms in the valence band, destabilized by the break of the Zr–O bond. The localized levels are energetically distributed so that severalphotons are able to excite the trapped electrons (see Fig. 7b). After photon excitation (see Fig. 7c) occurs the recombination process in which an electron of the conduction band lost their energy and reoccupies the energy levels of an electron and on hole in the valence band.

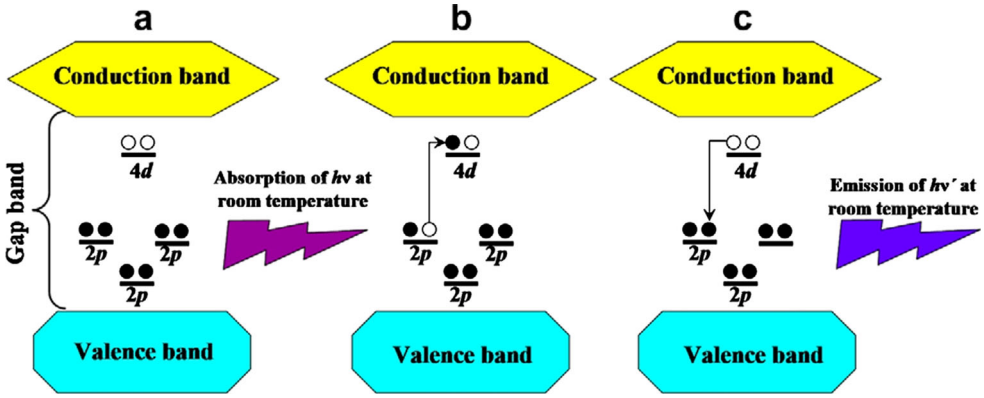

Fig. 7 Wide band model representation of a simple mechanism to explain the PL behavior of $BaZrO_3$ powders processed by the polymeric precursor method. **a** Before excitation, **b** excitation (formation of self-trapped excitons), and **c** after excitation [recombination of electron (e^-) hole (h·)

4 Conclusions

In summary, barium zirconate nanoparticles were prepared using the HTMW method, and their crystalline and optical properties were carefully investigated. The present synthesis process has low cost effectiveness and provides good phase purity at a low temperature synthesis. XRD patterns indicated that the crystallization process of the structurally disordered BZ clearly starts at a soaking time of 60 min and is completely ordered after 120 min. Raman spectra suggested the presence of different modes. FE-SEM has been used to follow the morphology on the different growth processes, and it is possible to gain a general view of the formation process. PL emission at room temperature can be related to the structural order–disorder in theBZO lattice, which is controlled by [ZrO_5] and [ZrO_6] clusters. The small band gap energy of disordered BZO powders can be associated with the presence of intermediary energy levels into the band gap and/or due to the charge discontinuities induced by the local disorder. These mechanisms are able to favor the trapping of electrons and holes during the excitation process and contribute to the PL emission. PL was clearly observed and has been systematically studied, providing more comprehensive knowledge on the types of defects generated by the different conditions during BZ growth.

Acknowledgments The financial support of this research project by the Brazilian research funding agencies CNPq 573636/2008-7, INCTMN 2008/57872-1 and FAPESP 2013/07296-2. We also gratefully acknowledged Laecio Cavalcante for Raman measurements.

References

1. H. Chaib, L.M. Eng, F. Schlaphof, Surface effect on the electrical and optical properties of barium titanate at room temperature. Phys. Rev. B **71**(2005), 085418-1–085418-13 (2005)
2. C. Wang, J. Hu, G.M. Chow, P.C. Hsu, Y.K. Hwu, Structural and optical properties of sol–gel-derived Au/$BaTiO_3$ nanocomposite thin films. J. Am. Ceram. Soc. **88**, 758–767 (2005)
3. E.J.H. Lee, F.M. Pontes, E.R. Leite, E. Longo, R. Magnani, P.S. Pizani, J.A. Varela, Effects of post-annealing on the dielectric properties of Au/BaTiO3/Pt thin film capacitors. Mater. Lett. **58**, 1715–1721 (2004)
4. A. Bergh, G. Craford, A. Duggal, R. Haitz, The promise and challenge of solid-state lighting. Phys. Today **54**, 42–47 (2001)
5. H.Y. Hwang, Perovskites: oxygen vacancies shine blue. Nat. Mater. **4**, 803–804 (2005)
6. D. Kan, T. Terashima, R. Kanda, A. Masuno, K. Tanaka, S. Chu, H. Kan, A. Ishizumi, Y. Kanemitsu, Y. Shimakawa, M. Takano, Blue-light emission at room temperature from Ar-irradiated $SrTiO_3$. Nat. Mater. **4**, 816–820 (2005)
7. A. Erb, E. Walker, R. Flukiger, $BaZrO_3$: the solution for the crucible corrosion problem during the single crystal growth of high-Tc superconductors $REBa_2Cu_3O_{7-\delta}$; RE = Y, Pr. Phys. C **245**, 245–251 (1995)
8. R. Liang, D.A. Bonn, W.N. Hardy, Growth of high quality YBCO single crystals using $BaZrO_3$ crucibles. Phys. C **304**, 105–111 (1998)
9. K.C. Goretta, E.T. Park, R.E. Koritala, M.M. Cuber, E.A. Pascual, N. Chen, A.R. de Arellano-Lopez, J.L. Routbort, Thermomechanical response of polycrystalline $BaZrO_3$. Phys. C **309**, 245–250 (1998)
10. S. Tao, J.T.S. Irvine, Conductivity studies of dense yttrium-doped $BaZrO_3$ sintered at 1325 & #xB0;C. J. Solid State Chem. **180**, 3493–3503 (2007)
11. S. Yamanaka, T. Hamaguchi, T. Oyama, T. Matsuda, S.I. Kobayashi, K.K. Kurosaki, Heat capacities and thermal conductivities of perovskite type $BaZrO_3$ and $BaCeO_3$. J. Alloys Compd. **359**, 1–4 (2003)
12. S. Yamanaka, K. Kurosaki, T. Maekawa, T. Matsuda, S.-I. Kobayashi, M. Uno, Thermochemical and thermophysical properties of alkaline-earth perovskites. J. Nucl. Mater. **344**, 61–66 (2005)
13. X.H. Liu, X.D. Wang, Preparation and luminescence properties of $BaZrO_3$:Eu phosphor powders. Opt. Mater. **30**, 626–629 (2007)
14. H. Zhou, Y. Mao, S.S. Wong, Shape control and spectroscopy of crystalline $BaZrO_3$ perovskite particles. J. Mater. Chem. **17**, 1707–1713 (2007)
15. L.S. Cavalcante, V.M. Longo, M. Zampieri, J.W.M. Espinosa, P.S. Pizani, J.R. Sambrano, J.A. Varela, E. Longo, M.L. Simões, C.A. Paskocimas, Experimental and theoretical correlation of very intense visible green photoluminescence in $BaZrO_3$ powders. J. Appl. Phys. **103**, 063527-1–063527-8 (2008)
16. C. Lee, W. Yang, R.G. Parr, Development of the Colle–Salvetti correlation-energy formula into a functional of the electron density. Phys. Rev. B **37**, 785–789 (1988)
17. A.D. Becke, Density functional thermochemistry. III. The role of exact exchange. J. Chem. Phys. **98**, 5648–5652 (1993)

18. V. Saunders, R. Dovesi, C. Roetti, R. Orlando, C.M. Zicovich-Wilson, N.M. Harrison, K. Doll, B. Civalleri, B. Bush, P.L.M. D'Arco, *CRYSTAL 03 user's manual* (University of Torino, Torino, 2003)
19. J. Muscat, A. Wander, N.M. Harrison, On the prediction of band gaps from hybrid functional theory. Chem. Phys. Lett. **342**, 397–401 (2001)
20. http://www.crystal.unito.it/Basis_Sets/Ptable.html
21. T.J.B. Holland, S.A.T. Redfern, Unit cell refinement from powder diffraction data: the use of regression diagnostics. Mineral. Mag. **61**, 65–77 (1997)
22. D.L. Wood, J. Tauc, Weak absorption tails in amorphous semiconductors. Phys. Rev. **5**, 3144–3151 (1972)
23. E. Orhan, J.A. Varela, A. Zenatti, M.F.C. Gurgel, F.M. Pontes, E.R. Leite, E. Longo, P.S. Pizani, A. Beltran, J. Andres, Room-temperature photoluminescence of $BaTiO_3$: joint experimental and theoretical study. Phys. Rev. B **71**, 085113-1–085113-7 (2005)
24. S. Parida et al., Structural refinement, optical and microwave dielectric properties of $BaZrO_3$. Ceram. Int. **38**, 2129–2138 (2012)
25. J. Rodriguez-Carvajal, Recent advances in magnetic structure determination by neutron powder diffraction. J. Phys. B **192**, 55–69 (1993)
26. M. Kara, K. Kurki-Suonio, Symmetrized multipole analysis of orientational distributions. Acta Crystallogr. **A37**, 201–210 (1981)
27. E. Prince, Comparison of profile and integrated-intensity methods in powder refinement. J. Appl. Crystallogr. **14**, 157–159 (1981)
28. K. Matsui, M. Ohgai, Formation mechanism of hydrous-zirconia particles produced by hydrolysis of $ZrOCl_2$ solutions: II. J. Am. Ceram. Soc. **83**, 1386–1392 (2000)
29. A. Singhal, G. Skandan, A. Wang, N. Glumac, B.H. Kear, R.D. Hunt, On nanoparticle aggregation during vapor phase synthesis. Nano Struct. Mater. **11**, 545–552 (1999)
30. P. Kubelka, F. Munk, Ein Beitrag zur Optik der Farbanstriche. Z. Tech. Phys. (Leipzig) **12**, 593–601 (1931)
31. P. Kubelka, New contributions to the optics of intensely light-scattering materials. Part I. J. Opt. Am. **38**, 448–457 (1948)
32. J. Tauc, R. Grigorovici, A. Vancu, Optical properties and electronic structure of amorphous germanium. Phys. Stat. Sol. **15**, 627–637 (1966)
33. A. Outzourhit et al., Characterization of hydrothermally prepared $BaTi_{1-x}Zr_xO_3$. J. Alloys Compd. **340**, 214–219 (2002)
34. S. Saha, S.B. Krupanidhi, Study of the electrical properties of pulsed laser ablated $(Ba_{0.5}Sr_{0.5})TiO_3$ thin films. Mater. Sci. Eng. B **57**, 135–146 (1999)
35. R.K. Roeder, E.B. Slamovich, Stoichiometry control and phase selection in hydrothermally derived $Ba_xSr_{1-x}TiO_3$ powders. J. Am. Ceram. Soc. **82**, 1665–1675 (1999)
36. S.B. Deshpande, Y.B. Khollam, S.V. Bhoraskar, S.K. Date, S.R. Sainkar, H.S. Potdar, Synthesis and characterization of microwave-hydrothermally derived $Ba_{1-x}Sr_xTiO3$ powders. Mater. Lett. **59**, 293–296 (2005)
37. A. Ries, A.Z. Simões, M. Cilense, M.A. Zaghete, J.A. Varela, Barium strontium titanate powder obtained by polymeric precursor method. Mater. Charact **50**, 217–221 (2003)
38. S. Komarneni, R. Roy, Q.H. Li, Microwave-hydrothermal synthesis of ceramic powders. Mater. Res. Bull. **27**, 1393–1405 (1992)
39. S. Komarneni, Q.H. Li, R. Roy, Microwave-hydrothermal processing of layered anion exchangers. J. Mater. Res. **11**, 1866–1869 (1996)
40. P.K. Dutta, J.R. Gregg, Hydrothermal synthesis of tetragonal barium titanate. Chem. Mater. **4**, 843–846 (1992)
41. V. Saunders, R. Dovesi, C. Roetti, R. Orlando, C.M. Zicovich-Wilson, N.M. Harrison, K. Doll, B. Civalleri, B. Bush, P.L.M. D'Arco, *CRYSTAL03 user's manual* (University of Torino, Torino, 2003)
42. H. Wang, J.J. Zhu, J.M. Zhu, X.H. Liao, S. Xu, T. Ding, H.Y. Chen, Preparation of nanocrystalline ceria particles by sonochemical and microwave assisted heating methods. Phys. Chem. Chem. Phys. **4**, 3794–3799 (2002)
43. G.J. Wilson, A.S. Matijasevich, D.R.G. Mitchell, J.C. Schulz, G.D. Will, Modification of TiO_2 for enhanced surface properties: finite Ostwald ripening by a microwave hydrothermal process. Langmuir **22**, 2016–2027 (2006)
44. Z. Lu, Y. Tang, L. Chen, Y. Li, Shape-controlled synthesis and characterization of $BaZrO_3$ microcrystal. J. Cryst. Growth **266**, 539–544 (2004)
45. Y.V. Kolenko, N.N. Oleinikov, A.A. Burukhin, A.S. Vanetsev, On the possibility of preparing fine-particle barium zirconate by hydrothermal synthesis. Inorg. Mater. **38**, 252–255 (2002)
46. J. Yoo, The effects of microstructure on $Ba_{1-x}Sr_xTiO_3$ pyroelectric materials for pyroelectric and bolometer infrared sensors, Ph.D. Thesis, University of Auckland, 1999
47. A.Z. Simões, E.C. Aguiar, A.H.M. Gonzalez, J. Andrés, E. Longo, J.A. Varela, Strain behavior of lanthanum modified $BiFeO_3$ thin films prepared via soft chemical method. J. Appl. Phys. **104**, 104115-1–104115-6 (2008)
48. A.Z. Simões, L.S. Cavalcante, C.S. Riccardi, J.A. Varela, E. Longo, Improvement of fatigue resistance on La modified $BiFeO_3$ thin film. Curr. Appl. Phys. **9**, 520–523 (2009)
49. S.-J.L. Kang, *Sintering densification, grain growth & microstructure* (Elsevier, Oxford, 2005), p. 265
50. M. Godinho, C. Ribeiro, E. Longo, E.R. Leite, Influence of microwave heating on the growth of gadolinium-doped cerium oxide nanorods. Cryst. Growth Des. **8**, 384–386 (2008)
51. J. Geng, Y. Lv, D. Lu, J.-J. Zhu, Sonochemical synthesis of $PbWO_4$ crystals with dendritic, flowery and star-like structures. Nanotechnology **17**, 2614–2620 (2006)
52. Y.B. Khollam, A.S. Deshpande, A.J. Patil, H.S. Potdar, S.B. Deshpande, S.K. Date, Microwave-hydrothermal synthesis of equi-axed and submicron-sized $BaTiO_3$ powders. Mater. Chem. Phys. **71**, 304–308 (2001)
53. M.L. Moreira, J. Andres, J.A. Varela, E. Longo, Synthesis of fine micro-sized $BaZrO_3$ powders based on a decaoctahedron shape by the microwave-assisted hydrothermal method. Crys. Growth. Design **9**, 833–839 (2009)